Impact of topographic obstacles on the discharge distribution in open-channel bifurcations

Emmanuel Jean Marie Mignot, C. Zeng, G. Dominguez, C.W. Li, N. Rivière, Pierre Henri Bazin

Author-produced version of the article published in Journal of Hydrology, 2013, vol. 494, p. 10-19
The original publication is available at http://www.sciencedirect.com/ doi : 10.1016/j.jhydrol.2013.04.023

IMPACT OF TOPOGRAPHIC OBSTACLES ON THE DISCHARGE DISTRIBUTION IN OPEN-CHANNEL BIFURCATIONS

Emmanuel Mignot*[1], Cheng Zeng[2], Gaston Dominguez[1], Chi-Wai Li[3], Nicolas Rivière[1] & Pierre-Henri Bazin[4]

[1]LMFA, CNRS-Universite de Lyon, INSA de Lyon, Bat. Joseph Jacquard, 20 avenue A. Einstein, 69621 Villeurbanne Cedex, France. Tel: 0033-4-72438070, Fax: 0033-4-72438718

[2]College of Water Conservancy and Hydropower Engineering, Hohai University, Nanjing 210098, P. R. China

[3]Department of Civil & Environmental Engineering, The Hong Kong Polytechnic University, Hong Kong

[4]Irstea, UR HHLY, 3 bis quai Chauveau CP220, 69336 LYON Cedex 09, France

* Corresponding author, E-mail: emmanuel.mignot@insa-lyon.fr

Abstract

When simulating urban floods, most approaches have to simplify the topography of the city and cannot afford to include the obstacles located in the streets such as bus stops, trees, parked cars, *etc*. The aim of the present paper is to investigate the error made when neglecting such singularities in a simple flooded 3-branch crossroad configuration with a specific concern regarding the error in discharge distribution to the downstream streets. Experimentally, the discharge distribution for 14 flows in which 9 obstacles occupying 1/6 of the flow section are introduced one after the other is measured using electromagnetic flow-meters. The velocity field for one given flow is obtained using horizontal-PIV. Additionally, all these flows are computed using a CFD methodology. It appears that the modification in discharge distribution is mostly related to the location of the obstacles with regards to the intersection, the location of the separating interface and is strongly impacted by the Froude number of the inflow while the influence of the normalized water depth remains very limited. Overall, the change in discharge distribution induced by the obstacles remains lower than 15% of the inflow discharge even for high Froude number flows.

Keywords

Subcritical open-channel flows, Bifurcation, Obstacles, Experimental, Numerical, Flooded urban streets.

1. Introduction

When an urban flood occurs, streets generally carry most of the flow from the upstream to downstream part of the city, especially when the area is densely urbanized (Mignot *et al.*, 2006). Flow in the streets is mostly 1D with mean velocities parallel to the building façades. However, in crossroads several flows collide and/or separate and the flow pattern becomes complex (see Mignot *et al.*, 2008) especially when artificial topographies create additional flow structures such as wakes, recirculation zones and secondary flows. Bazin *et al.* (2012) have studied the impact of obstacles on a junction flow where two subcritical flows collide. They observed that this impact depends on the location of the obstacles and may i) strongly modify the local velocity distribution and ii) the extensions of a recirculation zone. Moreover, the authors observed that if an obstacle is located within a recirculation zone, the impact of the obstacle is strongly damped.

Within street bifurcations, with a single inflow separating into two outflows, artificial topographies can also affect the flow distribution reaching the downstream streets. The aim of the present paper is thus to investigate i) the impact of obstacles on the local flow characteristics in bifurcation flows and ii) the consequences of such modifications of the flow pattern on the modification of flow distribution to the downstream branches. The selected artificial topographies are squared emerging obstacles which would represent trees, bus-stop or any other impervious urban furniture located near crossroads.

The general pattern of a steady subcritical 3-branch bifurcation without obstacle is described by Neary *et al.* (1999). A three-dimensional recirculating region develops in the lateral branch and secondary flows appear in both outlets. The principal challenge in such separating flow lies in the prediction of flow distribution from the incoming towards both outgoing flows. A review of analytical models developed to access such prediction is given by Rivière *et al.* (2007). The models are based on the momentum conservation law (see for instance Ramamurthy *et al.*, 1990), but Rivière *et al.* (2006) showed that this balance alone does not permit to calculate the flow distribution, and that additional equations must be introduced. These authors proposed an improved relationship based on i) the momentum conservation law from Ramamurthy *et al.* (1990), ii) suitable stage-discharge relationships for the downstream controls in the outflow channels and iii) an empirical correlation obtained through experimental data. This approach proved to accurately predict the flow distribution in three-branch bifurcations in ideal conditions: 90° angle, smooth walls and identical horizontal rectangular sections in each branch. Riviere *et al.* (2011) then generalized the results to 4-branch intersections.

Nevertheless, when singularities are introduced near or in the bifurcation, the flow pattern can be strongly affected and this analytical model obviously does not apply. The question raised by the present paper is to what extent an introduction of single or pairs of obstacles in the vicinity of the intersection affects the discharge distribution. Nine configurations of simplified square-shaped obstacles of typical size equal to 1/6 of the channel width are tested here. Their impact on the flow pattern and the downstream flow rates is analyzed for 14 flow configurations divided in 3 series.

For practical reasons, velocity field for all flow configurations with all obstacles could not be measured experimentally. The selected approach is rather based on a mix of experimental measurements and 3D calculations. After verification of their accuracy, these calculations are considered reliable enough to support the experimental investigation. In the first and second sections we describe the experimental and numerical methodologies respectively along with the selected flow and obstacle configurations. In a third section, we describe the impact of the obstacles on the flow pattern and discharge distribution and finally discuss the impact of the base flow (before introducing obstacles) characteristics on such results.

2. Experimental methodology

2.1 Experimental set-up

The experiments were performed in the channel intersection facility at the Laboratoire de Mécanique des Fluides et d'Acoustique (LMFA) at the University of Lyon (Insa-Lyon, France). The facility consists of three horizontal glass channels 2m long and b=0.3m wide each. The channels intersect at 90° with one upstream branch (with the flow rate Q_u), one downstream branch (flow rate Q_d) aligned with the upstream one and one lateral branch (flow rate Q_b). The upstream branch is connected to a large upstream storage tank where the flow is straightened and stabilized by passing through a honeycomb. The flow separates in the bifurcation and is finally collected by the downstream and lateral tanks. The lateral tank is connected to the downstream tank and the lateral discharge Q_b is measured using an electromagnetic flow-meter (see Figure 1). When pumped from the downstream tank to the upstream tank, the upstream flow-rate Q_u is measured using a second electromagnetic flow-meter. In order to control the flow conditions, PVC channels (length 60 cm) fitted with sharp crested weirs are added to the ends of the two exit channels so that L_d=L_b=2.6m while L_u=2m. A more detailed description of the experimental set-up can be found in (Rivière *et al.*, 2011).

For each flow configuration, the three boundary conditions to be set are: the upstream flow rate Q_u and the height of the sharp crest weirs C_d (for the downstream branch) and C_b (for the lateral branch). The stage

Author-produced version of the article published in Journal of Hydrology, 2013, vol. 494, p. 10-19
The original publication is available at http://www.sciencedirect.com/ doi : 10.1016/j.jhydrol.2013.04.023

discharge relationship (h_n,C_n,Q_n, n=b or d) is calibrated experimentally for each weir: h_b and h_d are measured using a digital point gauge at a length equal to 2 channel width upstream from the weirs. Similarly, the upstream water depth h_u used to characterize the upstream velocity and Froude number is measured one channel width upstream from the entry section of the bifurcation (see Figure 1). A point gauge is used to measure backwater curves in the main and the branch channel for most flow configurations.

Upstream water depth h_u ranges from 25 to 71 mm and discharge Q_u from 1.6 to 7.0 L/s. The corresponding Reynolds number ranges between 18000 and 65000 and the corresponding Froude number from 0.23 to 0.69. Moreover, the roughness height k_s was measured using a roughness meter which revealed that the maximum roughness is smaller than 1 μm and the average roughness smaller than 0.1 μm. Given the hydraulic diameter, ranging from D_h= 0.08m to 0.2m, the maximum relative roughness k_s/D_h is estimated to about 10^{-5}, corresponding to a hydraulically smooth regime in the Moody diagram.

2.2 Dimensional analysis and flow series

Dimensional analysis is applied to the present flow configuration. The 13 variables to be included in the dimensional analysis of discharge distribution law without obstacle are the channel width b and roughness k_s, the acceleration due to gravity g, the three flow rates and associated water depths Q_u and h_u, Q_b and h_b, Q_d and h_d, the two weir crest heights C_d and C_b and finally the fluid density ρ and dynamic viscosity μ.

5 available straightforward equations are:

- the mass conservation, which yields Q_u=Q_b+Q_d, permitting to remove the Q_d parameter.
- both calibrated stage discharge relationships (h_b,C_b,Q_b) and (h_d,C_d,Q_d), permitting to remove the C_b and C_d parameters.
- the momentum balance in the bifurcation along the main flow axis (x) as proposed by Ramamurthy *et al.* (1990) relating (h_u, h_d, Q_b) and thus permitting to remove the h_d parameter
- the empirical discharge distribution law proposed by Riviere *et al.* (2007) in their equation 2b which links the discharge distribution Q_b/Q_u with h_b through three parameters: $Q_d/(b.g.h_d^{3/2})$, h_d/b and h_b/h_d, thus permitting to remove h_b.

The 8 remaining variables are then b, g, Q_b, Q_u, h_u, k_s, ρ and μ including three scales, *i.e.* a time scale b^3/Q_u, a length scale b and a mass scale ρb^3.

Among the 5 final dimensionless parameters that rule the flow, two of them are discarded in this study. First one is the Reynolds number Re=$4\rho Q_u/[\mu(b+2h_u)]$, as its values are reasonably high (see section 2.1) to ensure fully turbulent flows. Second one is the dimensionless roughness height k_s/D_h, with D_h the hydraulic diameter. As the flow regime is hydraulically smooth (see section 2.1), effect of the roughness parameter is not considered hereafter.

The 3 final dimensionless parameters considered herein are then:

- the upstream Froude number F_u=Q_u/[b.h_u.(g.h_u)$^{0.5}$]
- the discharge distribution parameter R_q=Q_b/Q_u
- the normalized upstream water depth h_u/b

These three parameters govern the flow distribution in the 3-branch bifurcation without obstacle. In the sequel we investigate the impact of introducing obstacles in flows with varying value of each of these three parameters at a time. The flow configurations before introducing any obstacle are labeled “0” or “base” flow. Consequently, three series (S1, S2 and S3) of base flow configurations are considered in Table 1: S1 with varying F_{u0} and fixed R_{q0} and h_{u0}/b, S2 with varying R_{q0} and fixed h_{u0}/b and F_{u0} and S3 with varying h_{u0}/b and fixed R_{q0} and F_{u0}.

2.3 Obstacle configurations

For each base flow configuration (without obstacle) from Table 1, each obstacle is introduced one after the other near the bifurcation as shown on Figure 2. 10 obstacle configurations are considered for each flow: configuration labeled 0 is without obstacle (base); configurations labeled 1 to 7 comprise one obstacle; configurations labeled 8 and 9 comprise two obstacles (obstacles 2 + 4 for configuration 8 and 2 + 6 for configuration 9). The obstacles are square-shaped (section is 5x5cm), impervious, emerging (height is 20 cm), smooth blocks. They are led on the bottom and heavy enough to remain stable in the flow. They are located at a distance of 4 cm from the closest wall and junction section (as for obstacle 5 on Figure 2) except for obstacle 7 which is located at the center of the bifurcation.

2.4 Methodology

For each flow from Table 1:

- we adjusted the boundary conditions (C_d, C_b, Q_u) to obtain the desired base flow configuration without obstacle (labeled “0”).

- we measured the corresponding discharges Q_{b0}, Q_{d0} without obstacle as shown on Figure 1.

- we introduced each of the 9 obstacles one after the other without changing the boundary conditions (C_d, C_b, Q_u) and in each case, we measured the downstream discharges Q_{bi}, Q_{di}, with “i” the obstacle number.

- we computed the indicator of discharge distribution modification corresponding to the introduction of each obstacle $\Delta R_q=100.(R_{qi}-R_{q0})=100.(Q_{bi}-Q_{b0})/Q_u$, i=1…9.

This methodology thus permits to investigate i) the impact of each obstacle on the discharge distribution for each flow from Table 1 and ii) the evolution of such impact with the evolution of the characteristics of the base flow (F_{u0}, R_{q0} and h_{u0}/b).

2.5 Velocity fields measured through PIV

In addition to discharge measurements, the horizontal velocity field is measured using PIV at a selected elevation z=3cm for the flow configuration in bold in Table 1. This configuration is the slowest flow from the list and thus leads to the better measurement accuracy. Moreover, no PIV measurement could be performed using obstacle 7 as a large portion of the intersection would be in the shade of the obstacle.

Polyamid particles (50 μm diameter) are added to the water which re-circulates in our closed loop. A generator emmiting white light through a slot is used to create a plane, 5 mm thick, light sheet at the measurement elevation (z=3cm) in the channel junction and the branch channel. A 1280x1920 pixel progressive CCD-camera with 8 mm opening objective and 25ms time-exposure connected to a PC computer through a Firewire acquisition card is located above the free surface at an elevation of about 1.1 m. Inserting the whole set-up in the dark finally permits to record the particle motion at the lightened elevation at a fixed frame-rate of 30Hz during 133s. 4000 images are then recorded. The dimension of the measurement region is 350x500 mm with a horizontal resolution of 0.5 mm per pixel with 256 grey-levels. The commercial software Davis (from Lavision) permits to correct the optical distortions, to subtract the background and to compute each of the 4000 velocity fields over a 15x15 mm grid, that is about 20 points per channel section. The data is then averaged over the whole recording time to obtain the time-averaged velocity fields shown in Figure 5.

3. Numerical Simulation

3.1 Numerical method

In the numerical model, the 3D Unsteady Reynolds Averaged Navier-Stokes (URANS) equations for the conservation of mass and momentum of fluid are solved. The Reynolds stresses are represented by the eddy viscosity concept and the Spalart-Allmaras (SA) model is used for the turbulence closure. The σ-coordinate transformation is used to map the irregular domain with variable free-surface and bottom topography to a rectangular prism. A split-operator finite difference method with non-uniform rectilinear grid is employed to solve the governing equations. In each time interval, the equations are split into three steps: advection, diffusion and pressure propagation. In the advection step a characteristics-based scheme is used. In the diffusion step a centered difference scheme is used. In the pressure propagation step a Poisson equation is derived and solved by a stable and robust conjugate gradient method CGSTAB. A comparison of the velocity profiles in a bifurcation flow (without obstacle, measured by Barkdoll, 1997) computed by Li and Zeng (2009) using the present SA model and by Neary *et al*. (1999) using a k-ω model reveals that the two sets of results are quite similar. Further details of the present model can be found in (Lin and Li, 2002) and applications of the numerical model to flow division problems in open channels were performed by Li and Zeng (2010).

For the present application, the boundary conditions used are as follows. At the channel inlet the discharge Q_u is prescribed, the velocity profile is assumed uniform and the eddy viscosity profile is specified by using the mixing length model**,** the surface elevation gradient is set to zero and the pressure is assumed hydrostatic. At both channel outlets the water depth and the discharge are related by the experimental weir equations (h_b,C_b,Q_b) and (h_d,C_d,Q_d) and the streamwise gradients of the pressure and of the three velocity components are set to zero. At the free surface, the pressure is assumed atmospheric (zero relative pressure), the gradients of the velocity components are set to zero and the free surface elevation is tracked by solving the kinematic equation. At solid boundaries (channel walls and obstacles) the normal gradients of pressure and velocity are set to zero, and the velocity components along the boundaries are specified by the standard wall function, considering smooth walls. All 14 flow cases given in Table 1 with the base (no obstacle) and 9 obstacle configurations are replicated in the numerical simulation. The grid system used is rectilinear and non-uniform, with the finest grid size used near solid boundaries. The total number of grid points is 182160.

3.2 Validation of numerical method

A comparison between the computed and measured outlet discharges for all flow configurations using each obstacle configuration is given in Figure 3. The results are accurate, the difference between the computed and corresponding measured downstream outlet discharges is generally within 5% of the inlet discharge. This gives confidence regarding the model capacity to predict the flow distribution. Moreover, Figure 4 presents a comparison of measured and computed water depth evolution along the main channel for the reference flow configuration (see * in Table 1) without obstacle and with obstacle 7. The results are generally satisfactory and within 5% difference of the water depth. Nevertheless, the computed outlet water depth without obstacle is slightly higher than the measurements. Indeed, in the present case the downstream discharge is slightly overestimated by the calculation and thus, using the downstream stage-discharge relationship, the corresponding water depth is also overestimated. Overall, the tendency remains similar. Regarding the case with obstacle 7, the discharge distribution is fairly estimated and thus also the downstream backwater curve, but the computed head loss in the intersection is slightly lower than the measured one. Moreover, grid refinement study was carried out. The number of grid points used in the fine grid system was four times of that used in the original grid system. The corresponding computed backwater curves are shown in Fig. 4. The maximum difference between the two set of results is approximately 2%. The discharge distribution and the velocity profiles at various locations were also compared in Table 2. The difference in the discharge distribution is within 3%. Finally, the sensitivity of the solution to the inlet velocity profile was also studied: the replacement of the uniform velocity profile by a logarithmic profile only marginally affects the solution (see Figure 4), showing that the length of the upstream channel is sufficiently long to eliminate inlet effects.

Finally, a comparison of five measured and computed velocity field in the intersection region for the bold flow from Table 1 is included in Figure 5: without obstacle (O_0) and with obstacles 1, 2, 4, 5. As computed data results from unsteady numerical simulations, a time-averaging process was applied to the computed data for a better comparison with the time-averaged measured data. The magnitude of the velocity is generally satisfactorily predicted, except for the accelerated upstream flow near the right bank for obstacle 2. To conclude, the numerical model is considered as validated. In the sequel, the analysis of the impact of obstacles on the flow pattern is performed both from experimental and numerical data.

4. Results

Measured and computed velocities (Figure 5) and depths (Figure 6) reveal that the obstacles cause pile up of water immediate upstream and generate downstream wake regions with recirculating flows, leading to flow and streamline deflections. In the first subsection the impact of the obstacles on a selected flow ("PIV measured flow" in Table 1) is analyzed and in the three following sub-sections, the influence of the base flow characteristics from each serie in Table 1 on the obstacle impact is discussed.

4.1 Impact of the obstacles on the flow pattern and discharge distribution on a selected flow

Considering the PIV measured base flow (bold in Table 1) and using Figures 5, 6, 7 and 8, it is observed that:

- Without obstacle, the main flow is separated into two parts by the plane interface. The velocity along *x* axis thus decreases within the intersection. Maximum velocity along *y* axis is encountered in the lateral branch along the left bank wall while a recirculation zone is observed along the right bank wall. The water depth increases from the junction to the downstream branch while it decreases toward the lateral branch (see Figure 6). This behavior is in fair agreement with flow description in the literature by Neary *et al.* (1999)

- Introducing obstacle 1 strongly accelerates the right part of the upstream flow (-150mm>y>-300mm) in the section. Due to the increased momentum (inertia), the capacity of the flow to rotate towards the lateral branch is strongly reduced and the discharge in the lateral branch decreases (ΔR_q<0 in Figure 7).

- Introducing obstacle 2 deflects a large portion of the upstream flow towards the opposite wall (y=0) where it is accelerated. This reduces the flow entering the lateral branch (ΔR_q<0) and causes a reduction in the water depth in the lateral branch.

- Introducing obstacle 3 does not affect the flow pattern nor the discharge distribution as it is located within the very slow recirculation zone (dead zone, see Figure 8).

- Introducing obstacle 4 dramatically limits the section of the mean flow in the lateral branch near the downstream wall (0.2m<x<0.3m and -0.6m<y<-0.3m). The branch discharge is thus reduced (ΔR_q<0) and the flow pattern within the branch is also strongly modified.

- Introducing obstacles 5 and 6 limits the flow section in the downstream branch, causes pile-up of the junction water depth, which tends to increase the discharge in the lateral branch (ΔR_q>0).

- Introducing obstacle 7 tends to accelerate the flow along x axis within the junction on both sides of the obstacle (see Figure 8). The part of inflow deflected to the left bank (y>-150mm) reaches the downstream branch while the part deflected to the right bank is itself separated in two parts, each part reaching one outlet channel. The deflection towards right side enhances the flow reaching the lateral branch and thus leads to ΔR_q>0.

To conclude, it appears that both upstream obstacles (1 - 2) lead to ΔR_q<0 while both downstream obstacles (5 - 6) lead to ΔR_q>0. Oppositely, impact of both lateral obstacles (3 - 4) on ΔR_q differs. Moreover, Figure 7 reveals that the impact of introducing obstacle configurations 8 (resp. 9) is about the sum of the impacts of the constituting obstacles, that is of obstacles 2+4 (resp. 2+6).

4.2 Impact of the inflow Froude number: F_{u0} (Serie 1)

Figure 7 reveals that the sign (positive or negative) of ΔR_q for a given obstacle does not change with varying Froude number of the base flow: none of the curves crosses the ΔR_q=0 axis. It appears that as the Froude number of the base flow increases, the impact of each obstacle raises: $|\Delta R_q|$ increases. Indeed, the Froude number is the square root of the ratio between inertia force and gravity force. So, as the resistance force (drag force) produced by the flow on an obstacle is proportional to the square of the flow velocity, the increase in flow inertia leads to an increased resisting force on the obstacles. In return, as the Froude number of the flow increases, the pile-up at the stagnation point in front of the obstacle and the intensity of the wake increase. Both processes affect the flow pattern and thus the obstacle impact is enhanced. Moreover, Figure 7 reveals that for the flows studied in Serie 1, magnitude of discharge distribution modification ranges between less than 5% for the low Froude number configurations to a maximum of 10% for the highest Froude number. Modifications are then limited for all flow and obstacle configurations.

4.3 Impact of the base discharge distribution: R_{q0} Series 2

Figures 8 and 9 show the impact of introducing obstacles in flows which base discharge distribution R_{q0} (without obstacle) varies between 0.2 and 0.8. Experimentally, increasing R_{q0} with constant F_{u0} and h_{u0}/b is obtained by keeping the same upstream discharge Q_u and water depth h_u and by increasing (resp. decreasing) the weir crest height in the downstream channel C_d (resp. branch C_b). Thus for constant upstream flow conditions, varying R_{q0} affects (see Figure 8): i) the location of the interface-plane which separates the upstream flow into a left portion reaching the downstream branch and a right portion reaching the lateral branch, ii) the width of the recirculation region in the branch and iii) the tendency of the downstream flow to detach from the left bank (y=0) and to initiate a recirculation zone in the downstream branch. Assuming a 2D flow, the interface between both inflows starts in the upstream branch and ends at the downstream corner of the junction. For R_{q0}=0.5, the upstream limit of the interface plane is located at the centerline of the upstream branch (x<0, y=-b/2), while for R_{q0}<0.5 this plane starts at y<-b/2 and for Rq_0>0.5, it starts at y>-b/2. Tendencies of ΔR_q for increasing R_{q0} with the nine obstacles are summarized in Table 3. The relative location of this interface and each obstacle permits to explain most results:

- For low R_{q0}, the interface is located near the lateral branch side and thus far from **obstacle 1**. As obstacle 1 then tends to accelerate the flow, its rotation capacity towards the lateral branch decreases: ΔR_q<0 (see section 4.1). For increasing R_{q0}, the interface starts closer to obstacle 1 and part of upstream flow deflected to the right side of the obstacle passes to the right side of the interface of the base flow and finally reaches the lateral branch. Consequently, the ΔR_q<0 tendency described above decreases as R_{q0} increases.

- Oppositely, as R_{q0} increases the interface plane goes away from **obstacle 2** and the discharge distribution becomes less influenced by the obstacle: |ΔR_q| decreases. It should be noted that for very low R_{q0}, the base flow interface plane becomes located very close to the right bank of the inflow and thus the part of the flow deflected by obstacle 2 to the right side of the inflow leads to an increase of ΔR_q compared to slightly higher R_{q0} (see Figure 9).

- **Obstacle 4** is located in the major flow zone of the branch channel. Its blockage effect increases with the lateral outflow discharge, that is as R_{q0} increases.

- O**bstacles 5 and 6** tend to block the flow in the downstream channel and thus to increase the branch discharge (see section 4.1). However, for increasing R_{q0} values, the discharge in the downstream channel decreases and thus also the velocity at this section. Corresponding pile-up and adverse pressure gradient thus decreases. Consequently, introducing obstacles 5 and 6 always leads to $\Delta R_q>0$ but this impact decreases as R_{q0} increases.

- For R_{q0} lower or close to 0.5, **obstacles 7** tends to deflect most of the right part of upstream flow towards the branch side leading to $\Delta R_q>0$ (see section 4.1 and Figure 8). At the same time, the acceleration in the downstream channel suppresses the flow separation at the left bank. However, for R_{q0} much larger than 0.5, part of the flow which reached the lateral branch when no obstacle was included is now deflected by obstacle 7 towards the left wall (y=0) and finally reaches the downstream channel. As a consequence, for very high R_{q0}, obstacle 7 benefits the downstream channel and $\Delta R_q<0$.

- **Obstacle configurations 8 and 9** follow the same trend as their constitutive obstacles (2+4 for obstacle 8 and 2+6 for obstacle 9).

- The impact of **obstacle 3** is related to the recirculation width in the lateral branch. According to Figure 8, as R_{q0} increases, the width of the recirculation region in the lateral branch decreases and thus **obstacle 3** tends to pass from the recirculation zone to the main flow. As a consequence, for high R_{q0}, obstacle 3 tends to block off part of the lateral branch flow (increasing the water depth and creating and adverse pressure gradient), leading to $\Delta R_q<0$.

4.4 Impact of the normalized water depth: h_{u0}/b (Serie 3)

Figures 10 and 11 show the influence of the upstream water depth of the base flow h_{u0} on the impact of each obstacle. First, it appears that the effect of water depth on the change in flow distribution is negligible except for the 3 configurations involving obstacle 2 (configurations 2, 8 and 9) where it still remains limited. For these configurations, as the base water depth increases (with similar Froude number and discharge distribution), the discharge in the branch is reduced: $\Delta R_q<0$ decreases until a minimum value for h_{u0}/b~0.18 and then increases again for higher water depths. Numerical results in Figure 10 show that varying the water depth h_{u0} affects the wakes generated downstream from obstacles 1 and 2, even though all our experiments belong to the "vortex street" flow type, when following Chen & Jirka (1995) approach. Indeed, the wake parameter $S=f.a/(4h_u)$ ranges from 0.003 to 0.013 (*i.e.* $S<0.2$), with a=0.05m the obstacle width and f the Darcy-Weisbach coefficient ranging from 0.02 to 0.027 considering smooth walls in our experiments. For obstacle 1, the wake modification hardly affects the discharge distribution (see Figure 11) as the obstacle is located far from the separation streamline. Oppositely, for obstacle 2, the wake modification appears to be responsible for the modification in discharge distribution for configurations 2, 8 and 9. This information revealed by the numerical results proves the interest of coupling experimental and numerical data for the analysis.

5. Discussion and Conclusion

The aim of the present paper was to investigate how the flow is affected by obstacles located in a 3-branch bifurcation with specific attention towards the impact on the discharge distribution to the downstream branches. Two types of measurements were undergone: i) discharge distribution measurements for 14 flows belonging to three series in which only one main parameter of the flow was varying at a time and in which 9 obstacles were introduced one after the other; and ii) horizontal velocity field for one selected flow with most obstacle configurations using PIV techniques. In parallel all flows with all obstacle cases were computed using a CFD approach. Combination of both experimental and numerical approaches permitted to explain the outlet discharge modifications induced by obstacles by analyzing the changes in the flow pattern. The following conclusions can be outlined:

- The computation results of the numerical model in terms of outlet discharges and flow field are in fair agreement with measurements and thus this CFD model represents a suitable predictive tool to further study localized urban flooding configurations where the flow is strongly complex and 3D.
- The impact of an impervious obstacle on the discharge distribution in a subcritical 3-branch bifurcation flow is strongly dependent on the location of the obstacle with regards to the intersection. Obstacles located within the upstream branch increase the streamwise flow velocity and thus tend to reduce the lateral and increase the downstream discharge (Rq_0 decreases up to 12%). Oppositely obstacles located within the downstream branch tend to block off the flow in this branch and to reduce the corresponding discharge while increasing the lateral discharge (Rq_0 increases up to 3%). Finally for obstacles located within the lateral branch, their impact depends on the side of the channel in which they are introduced: i) towards the downstream wall of the lateral branch, they tend to block off the lateral flow and thus promote the

downstream and reduce the lateral discharge (Rq_0 decreases up to 4.5%); ii) towards the upstream wall, the obstacle is usually located within the recirculation zone where it has no impact but as the width of this zone reduces, the obstacle can block off part of the lateral discharge (Rq_0 decreases up to 3%). Such influence of the location of the obstacles on the modifications of discharge distribution should be considered in flooded urban areas for car park planning. Moreover, for a given obstacle, as the Froude number of the inflow increases, the impact of the obstacle strongly increases. Oppositely, it appeared that the water depth in the intersection has very limited influence on the impact of obstacles.

- For a given flow in which an obstacle is introduced, the impact on the discharge distribution is a direct consequence of the modifications of the following flow structures: i) streamwise and centrifugal flow acceleration, ii) width of the recirculation zone and iii) wake downstream the obstacle.

- Overall, the impact of the obstacles remains limited to about 10 to 15% of the inflow discharge even for very high Froude number flows. However, considering a scale ratio of about 25 between the experimental set-up and a real street (leading to a 7.5m wide street) and using a Froude similarity, the equivalent velocity would reach 1 to 2 m/s and the Reynolds number $2x10^6$ to $8x10^6$. Assuming a typical street roughness height of 5 mm, the flow regime at the street scale will be hydraulically rough which may introduce some discrepancies when transferring the present results to real urban flood cases. Moreover, this impact is expected to increase with the size of obstacles, which is not covered in the present study. For flooding consideration, 10% to 15% change can be substantial. It is recommended to include these singularities as impervious areas within the topography of a city in 3D or 2D urban flood simulation or by a calibrated head loss term in 1D network simulation.

5. Acknowledgements

The work was supported by a grant from the PROCORE-France/Hong Kong Joint Research Scheme sponsored by the Research Grants Council and the Consulate General of France in Hong Kong (2011, project n°24664RB) and benefited from the support of the French CNRS, INSU, through grant EC2CO Cytrix 2011-231.

6. References

Barkdoll, B.D., 1997. Sediment control at lateral diversions, PhD dissertation, Civil and Environmental Engineering, University of Iowa, Iowa City, Iowa.

Bazin, P.H., Bessette, A., Mignot, E., Paquier, A., Riviere, N., 2012. Influence of detailed topography when modeling flows in street junction during urban flooding. Journal of Disaster Research, 7 (5), 560-566.

Chen, D., Jirka, G.H., 1995. Experimental study of plane turbulent wakes in shallow water layer. Fluid Dynamics Res. 16 (1), 11-41.

Li, C.W., Zeng, C., 2009. 3D Numerical modelling of flow divisions at open channel junctions with or without vegetation, Advances In Water Resources, 32, 1, 49-60.

Li, C.W., Zeng, C., 2010. Flow division at a channel crossing with subcritical or supercritical flow. Intern. J. for Num. Methods in Fluids. 62, 56-73.

Lin, P., Li, C.W., 2002. A sigma-coordinate three-dimensional numerical model for surface wave propagation. International Intern. J. for Num. Methods in Fluids. 38, 1045-1068.

Mignot, E., Paquier, A., Ishigaki, T., 2006. Comparison of numerical and experimental simulations of a flood in a dense urban area. Water Science and Tech. 54, 65–73.

Mignot, E., Riviere, N., Perkins, R.J., Paquier, A., 2008. Flow patterns in a four branches junction with supercritical flow. J. Hydr. Eng. 134(6), 701–713.

Neary, V.S., Sotiropoulos, F., Odgaard, A.J., 1999. Three-dimensional numerical model of lateral-intake inflows. J. Hydr. Eng. 125(2), 126–140.

Ramamurthy, A.S., Tran, D.M., Carballada, L.B., 1990. Dividing flow in open channels. J. Hydr. Eng. 116(3), 449–455.

Rivière, N., Perkins, R.J., Chocat, B., Lecus, A., 2006. Flooding flows in city crossroads: 1D modelling and prediction. Water Science and Techn. 54(6-7), 75–82.

Riviere, N., Travin, G., Perkins, R.J., 2007. Transcritical flows in open channel in tersections. 32nd IAHR Congress, 1-6 July 2007, Venice, Italy.

Riviere, N., Travin, G., Perkins, R.J., 2011. Subcritical open channel flows in four branch intersections. Water Resources. Res. 47, W10517.

Author-produced version of the article published in Journal of Hydrology, 2013, vol. 494, p. 10-19
The original publication is available at http://www.sciencedirect.com/ doi : 10.1016/j.jhydrol.2013.04.023

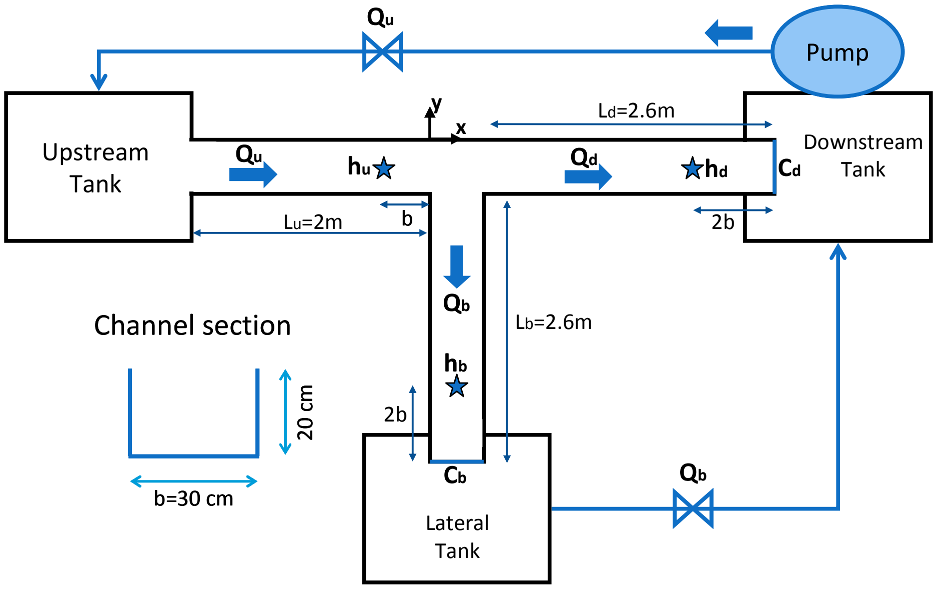

Figure 1: Scheme of the experimental set-up.

Author-produced version of the article published in Journal of Hydrology, 2013, vol. 494, p. 10-19
The original publication is available at http://www.sciencedirect.com/ doi : 10.1016/j.jhydrol.2013.04.023

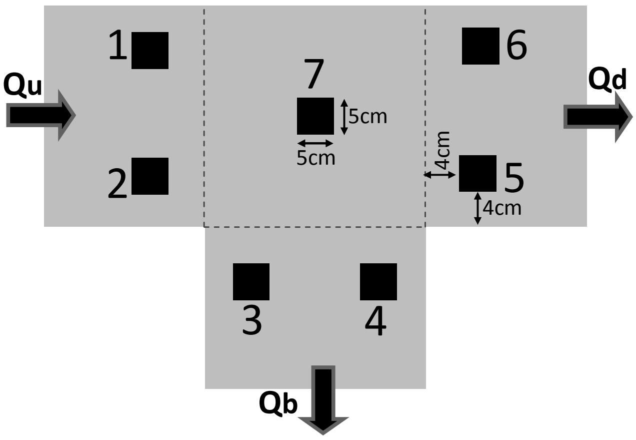

Figure 2: Location of the obstacles around the bifurcation.

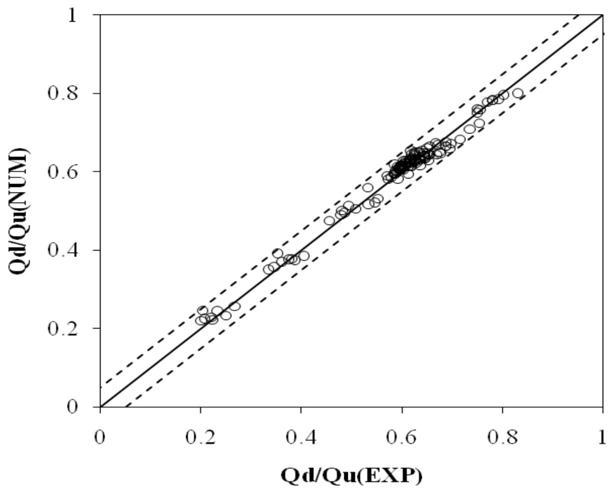

Figure 3: Comparison between measured (M) and computed (C) discharge ratios for the 14 flow x 10 obstacle configurations. Dotted lines refer to +/- 5% of Q_u

Author-produced version of the article published in Journal of Hydrology, 2013, vol. 494, p. 10-19
The original publication is available at http://www.sciencedirect.com/ doi : 10.1016/j.jhydrol.2013.04.023

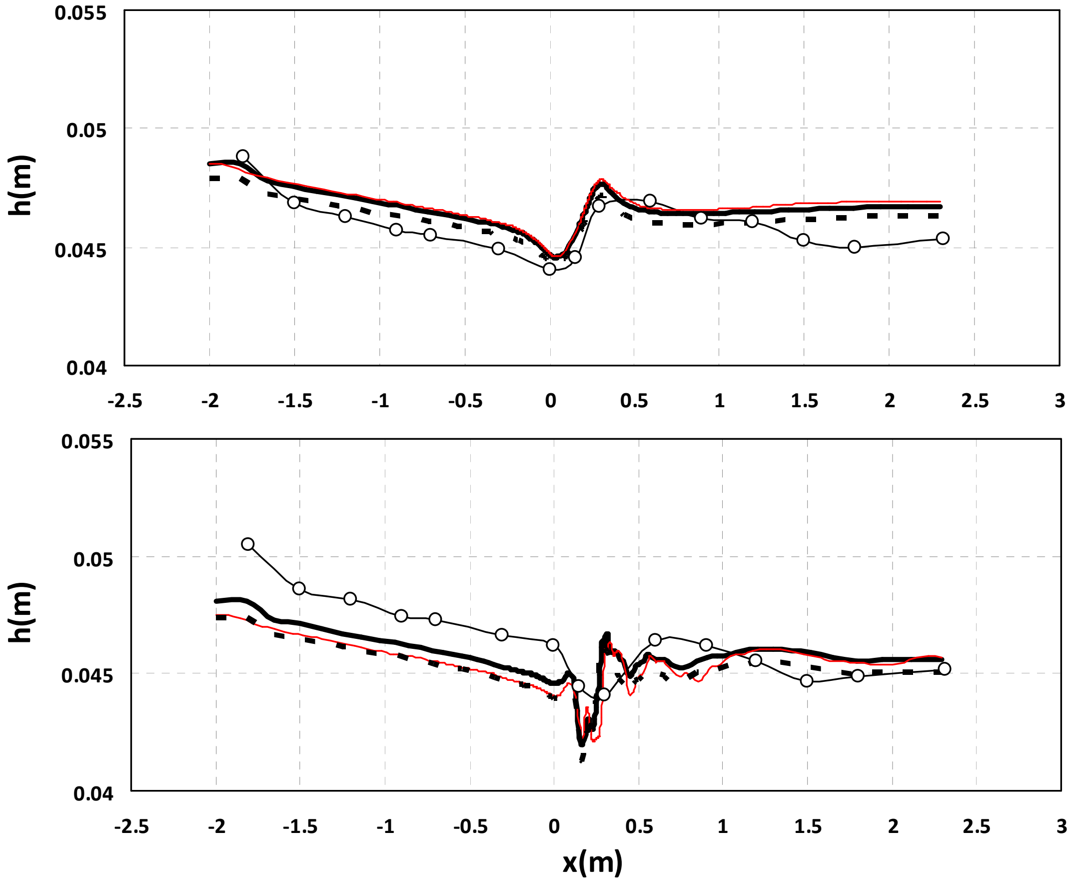

Figure 4: Measured (symbols) and computed backwater curves for the reference flow configuration (* in Table 1) along the main channel at y=-0.22m without obstacle (O0, top) and with obstacle 7 (O7, bottom) using the reference numerical configuration (plain thick line), the refined mesh (red line) and the reference configuration with log profile at the inlet (dotted line).

Author-produced version of the article published in Journal of Hydrology, 2013, vol. 494, p. 10-19
The original publication is available at http://www.sciencedirect.com/ doi : 10.1016/j.jhydrol.2013.04.023

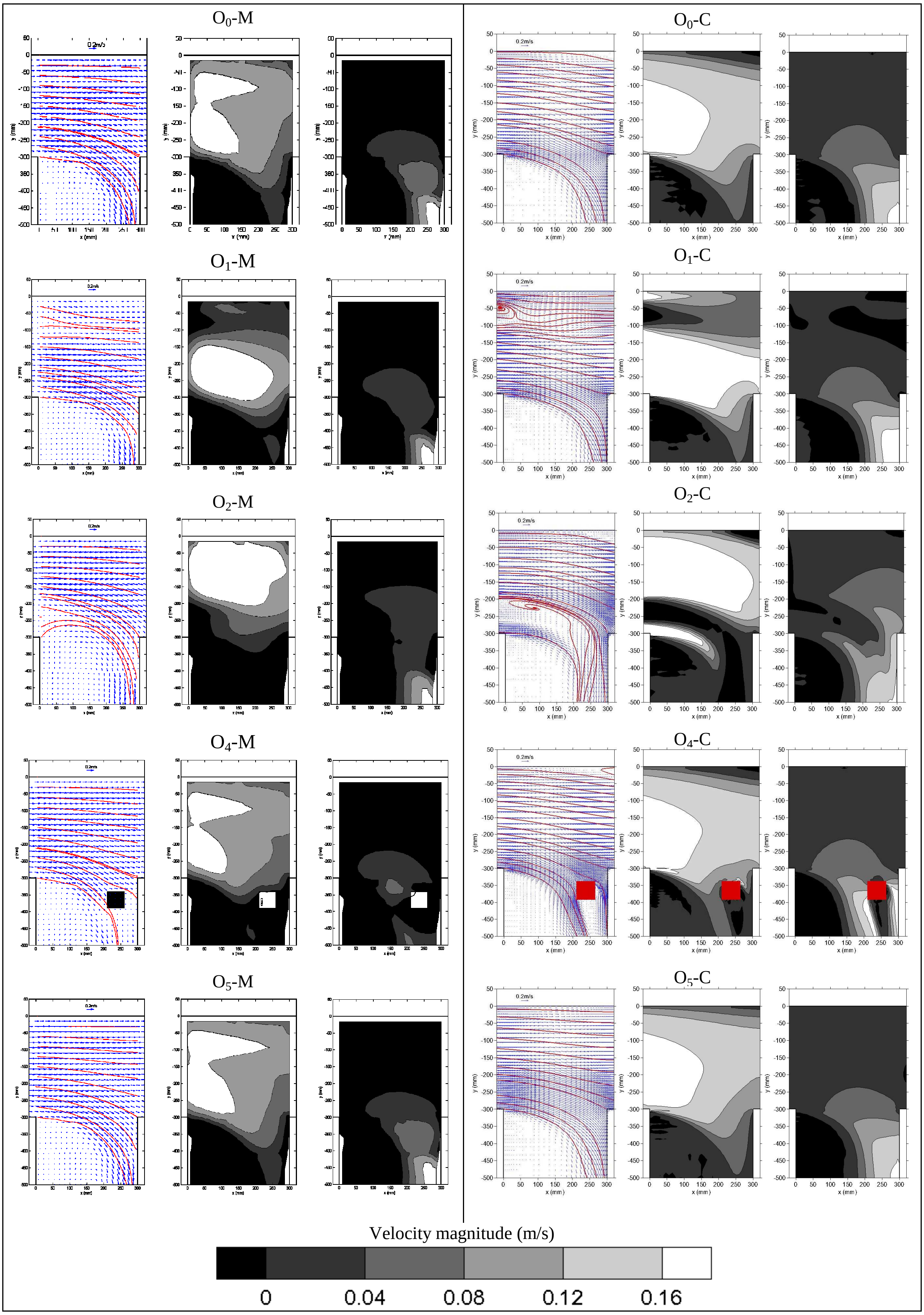

Author-produced version of the article published in Journal of Hydrology, 2013, vol. 494, p. 10-19
The original publication is available at http://www.sciencedirect.com/ doi : 10.1016/j.jhydrol.2013.04.023

Figure 5: Measured (M) and Computed (C) velocity fields at z=3cm for bold flow in Table 1 without obstacle (O_0) and with obstacle configurations 1, 2, 4, 5. For each flow: left graph = velocity field with streamlines; center graph = u time-averaged velocity (along x axis); right graph= v time-averaged velocity (along y axis).

Author-produced version of the article published in Journal of Hydrology, 2013, vol. 494, p. 10-19
The original publication is available at http://www.sciencedirect.com/ doi : 10.1016/j.jhydrol.2013.04.023

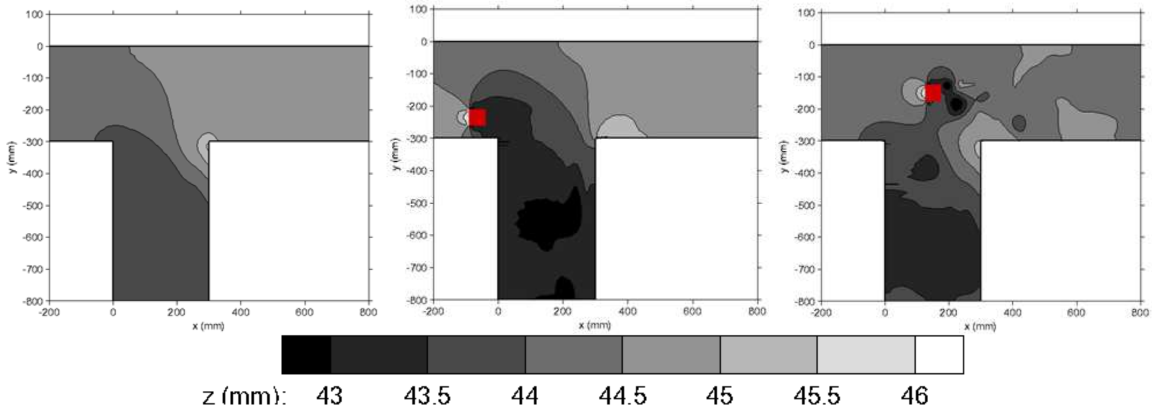

Figure 6: Computed free-surface elevation fields for bold flow in Table 1 without obstacle (O0) and with obstacles O2 and O7.

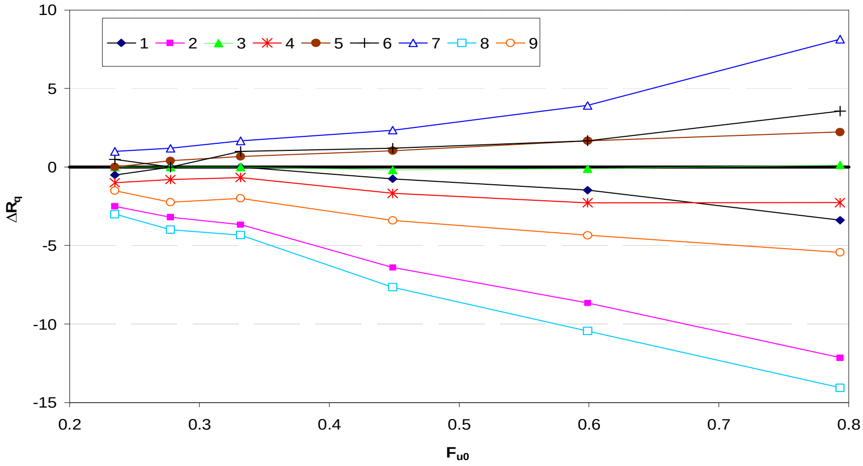

Figure 7: Measured impact of obstacles on the discharge distribution for flows in Serie 1 from Table 1 with varying base upstream Froude numbers F_{u0}.

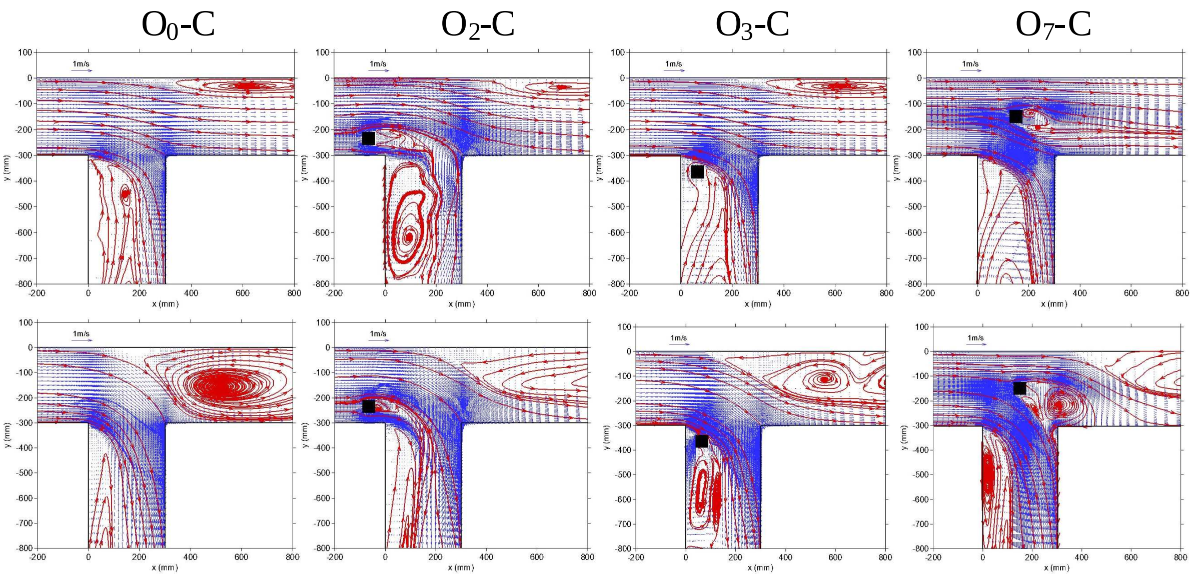

Figure 8: Computed velocity fields at z=3cm with obstacle configurations 0, 2, 3 and 7 for R_{q0}=0.39 (top) and R_{q0}=0.8 (bottom) in Serie 2 from Table 1.

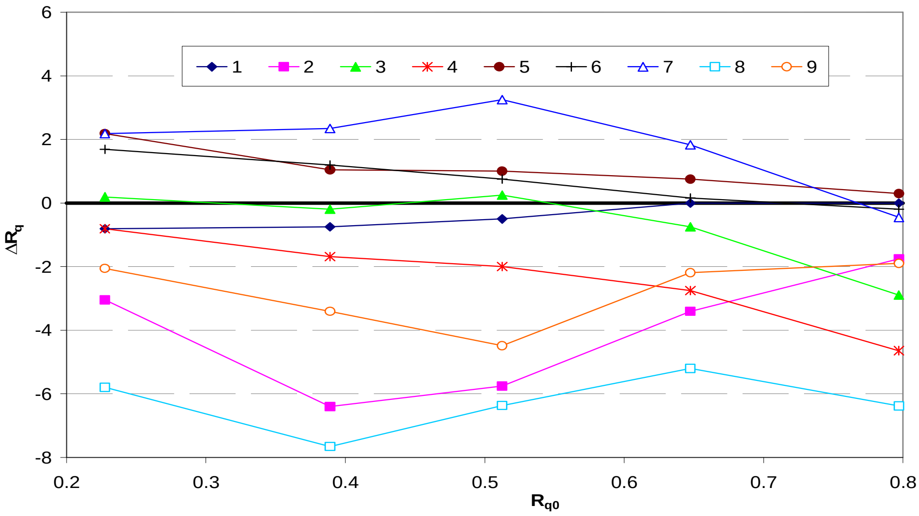

Figure 9: Measured impact of obstacles on the discharge distribution for flows in Serie 2 from Table 1 with varying base discharge distribution R_{q0}

Author-produced version of the article published in Journal of Hydrology, 2013, vol. 494, p. 10-19
The original publication is available at http://www.sciencedirect.com/ doi : 10.1016/j.jhydrol.2013.04.023

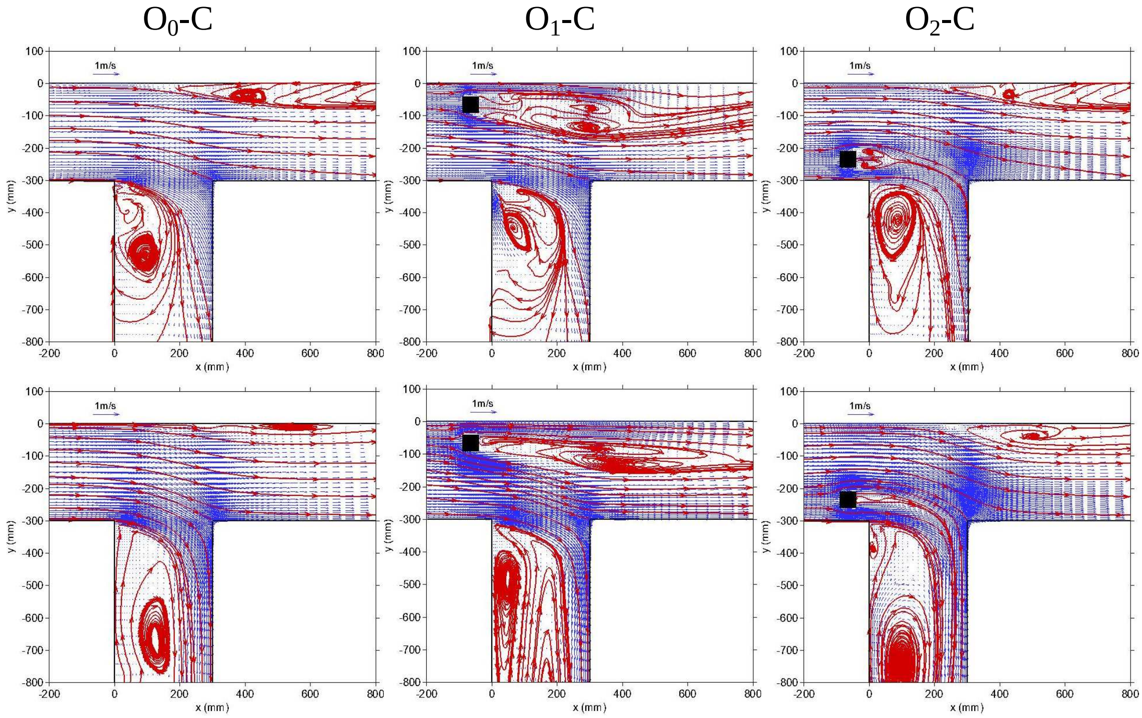

Figure 10: Computed velocity fields with obstacle configurations 0, 1 and 2 for h_{u0}/b=0.08 (top) and h_{u0}/b=0.22 (bottom) in Serie 3 from Table 1.

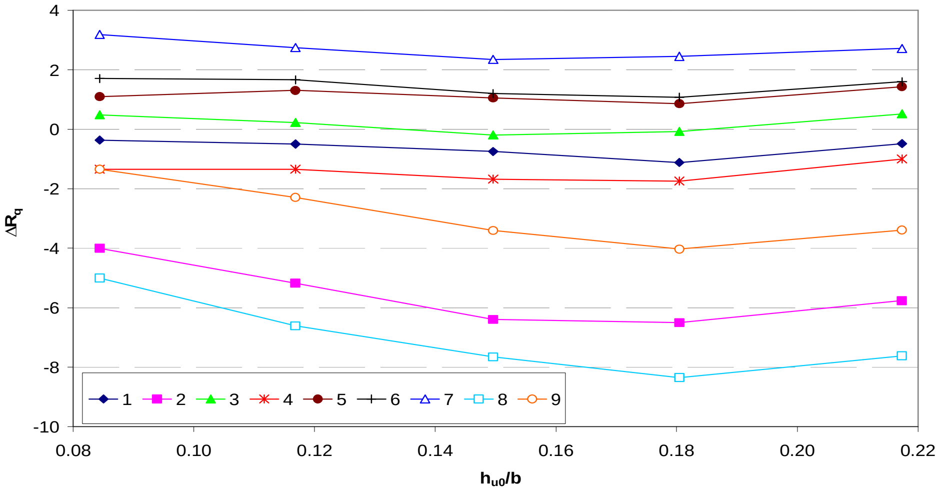

Figure 11: Measured impact of obstacles on the discharge distribution for flows in Serie 3 from Table 1 with varying base upstream water depths h_{u0}/b

Author-produced version of the article published in Journal of Hydrology, 2013, vol. 494, p. 10-19
The original publication is available at http://www.sciencedirect.com/ doi : 10.1016/j.jhydrol.2013.04.023

Table 1: Non-dimensional parameters of the 14 flow configurations. The flow marked with an asterisk * (common to the three series) is referred to as the "reference configuration". The first flow in bold, selected for velocity field measurement, is referred to as "PIV measured flow".

Serie #	R_{a0}	F_{u0}	h_{u0}/b
S1	**0.38**	**0.23**	**0.14**
	0.40	0.28	0.15
	0.39	0.33	0.15
	0.39*	0.45*	0.15*
	0.39	0.60	0.14
	0.39	0.79	0.13
S2	0.23	0.44	0.15
	0.39*	0.45*	0.15*
	0.51	0.45	0.15
	0.65	0.44	0.15
	0.80	0.45	0.15
S3	0.40	0.44	0.08
	0.38	0.45	0.12
	0.39*	0.45*	0.15*
	0.39	0.45	0.18
	0.39	0.45	0.22

Author-produced version of the article published in Journal of Hydrology, 2013, vol. 494, p. 10-19
The original publication is available at http://www.sciencedirect.com/ doi : 10.1016/j.jhydrol.2013.04.023

Table 2 Grid refinement study of discharge distribution for the reference flow configuration (* in Table 1).

No obstacle	Q_u (L/s)	R_q	h_u (mm)	h_d (mm)	h_b (mm)
Original	4	0.355	45.9	47.7	44.6
Fine grid	4.02	0.353	45.9	47.7	43.7

Author-produced version of the article published in Journal of Hydrology, 2013, vol. 494, p. 10-19
The original publication is available at http://www.sciencedirect.com/ doi : 10.1016/j.jhydrol.2013.04.023

Table 3: Evolution of ΔR_q as R_{q0} increases (Serie S2)

Obstacle #	Low R_{q0} : sign of ΔR_q (Fig.8)	Evolution of ΔR_q as R_{q0} ↑ (Fig.10)
1	**<0**	→ **0**
2	**<0**	→ **0**
3	**≈0**	$\Delta R_{q3}<0$
4	**<0**	$\Delta R_{q4}<<0$
5-6	**>0**	→ **0**
7	**>0**	→ **0***
8	**<0**	**≈**
9	**<0**	→ **0**

*ΔR_{q7} becomes negative for $R_{q0}\geq0.8$